ACS APPLIED MATERIALS & INTERFACES

RESEARCH ARTICLE

www.acsami.org

Intelligent Hydrated-Sulfate Template Assisted Preparation of Nanoporous TiO_2 Spheres and Their Visible-Light Application

Xujie Lü,[†,§] Fuqiang Huang,[*,†] Jianjun Wu,[†,§] Shangjun Ding,[†,§] and Fangfang Xu[‡]

[†]State Key Laboratory of High Performance Ceramics and Superfine Microstructures and [‡]Inorganic Materials Analysis and Testing Center, Shanghai Institute of Ceramics, Chinese Academy of Sciences, Shanghai 200050, P.R. China

[§]Graduate School of the Chinese Academy of Sciences, Beijing 100049, P.R. China

Supporting Information

ABSTRACT: Hydrated metal sulfates ($MSO_4 \cdot xH_2O$, M = Zn, Fe, Co, Mg, etc.) were proposed to be intelligent templates to solvothermally synthesize nanoporous TiO_2 spheres with tunable chamber structures from hollow to solid and hybrid compositions. During the reaction, hydrated sulfate serves simultaneously as spherical template, water supplier, and composition controller, and it can be easily removed by washing. The as-prepared anatase TiO_2 spheres were evidenced to contain highly crystallized TiO_2 nanocrystals hybridized with a small amount of metal oxide from the hydrated sulfate. The formation mechanism of the hollow spheres involves the self-conglobation of hydrated sulfate, the hydrolysis of tetrabutyl titanate on the spherical templates, and the subsequent process of solvothermal crystallization. The proposed hydrated-sulfate assisted solvothermal (HAS) strategy was demonstrated to be widely applicable to various systems. When applied to visible-light photocatalysis, the hybrid TiO_2 spheres exhibit excellent photocatalytic performance, benefiting from the reduced charge recombination rate contributed by the heterojunctions of TiO_2 and the hybridized metal oxides.

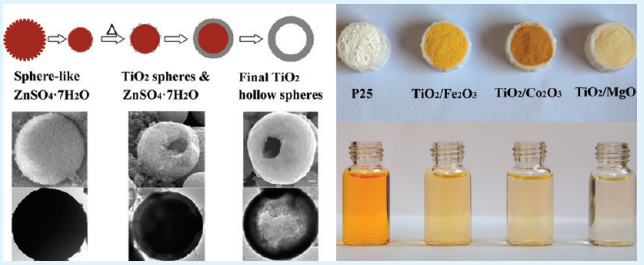

KEYWORDS: intelligent template, nanoporous TiO_2 spheres, hydrated sulfates, solvothermal strategy, visible-light applications, photocatalysis

1. INTRODUCTION

Titanium(IV) dioxide (TiO_2), as one of the most important transition-metal functional oxides, has attracted extensive attention during the past decades for its superior physical and chemical properties. Many potential applications such as efficient photocatalysts and electrode materials for dye-sensitized solar cells (DSCs) have been extensively investigated.[1,2] To utilize solar energy efficiently, TiO_2 should be well-crystallized with a high surface area to ensure abundant active sites and outstanding dye adsorption ability and should have outstanding charge separation and transport efficiencies.[3] In this respect, micrometer-sized porous spheres of TiO_2 nanocrystallites are beneficial, owing to their large surface area, unique optical properties allowing light trapping, and ease of recovery (for example, by sedimentation) in practical applications.[3]

Currently, the general synthetic strategy for the preparation of hollow spheres is the utilization of templates, including "hard" ones, such as polymers,[4,5] silica,[6] carbon,[7] and metallic cores,[8] as well as "soft" ones, for instance, emulsion droplets,[9] micelles,[10] microfluid,[11] and gas bubbles.[12,13] These reported methods, although easily implemented, however, are incapable to readily tune the interior structures and the compositions. Therefore, it is highly desirable to develop a novel synthesis method using an intelligent template, which (i) is the water supplier for hydrolysis reaction, (ii) can control the structures and compositions by simply adjusting the reaction conditions, (iii) has a broad scope of application, (vi) is easily removed from the final products, and (v) is earth-abundant and environmentally benign.

To satisfy all of these favorable requirements, in our recently published communication,[14] we have fabricated hollow spheres of TiO_2/ZnO composite structure via a solvothermal reaction assisted by $ZnSO_4 \cdot 7H_2O$. To understand this method well, herein, the systematic investigation was conducted and the hydrated-sulfate assisted solvothermal (HAS) strategy is found to be a facile and general strategy to fabricate nanoporous TiO_2 spheres with tunable chamber structures and hybrid compositions. The TiO_2 spheres prepared using $ZnSO_4 \cdot 7H_2O$ are firstly demonstrated as an example to illustrate this strategy, followed by other hydrated sulfates with different compositions ($FeSO_4 \cdot 7H_2O$, $CoSO_4 \cdot 7H_2O$, $MgSO_4 \cdot 7H_2O$, etc.).

In this study, the evolution of intelligent spherical templates of hydrate sulfates, the growth mechanism of TiO_2 spheres, the

Received: November 18, 2010
Accepted: December 22, 2010
Published: January 12, 2011

controllable preparation of structures and compositions, the generality of the HAS strategy in various systems, and their visible-light application are going to be further clarified. Interestingly, it is after being stirred in ethanol that irregular hydrated sulfate powders can be converted into spherical templates. Afterwards, the metallorganic Ti source reacts with the water that is slowly released from the surface of spherical hydrated sulfate to form TiO_2 nanocrystals with the desired spherical structure. This strategy provides a simple intelligent-template assisted approach for cost-effective preparation of TiO_2 spheres with controllable structures and compositions. When used in organic pollutant degradation, as-prepared hybrid TiO_2 spheres (TiO_2/Fe_2O_3, TiO_2/Co_2O_3, TiO_2/MgO, etc.) exhibit good photocatalytic activities under visible-light irradiation.

2. EXPERIMENTAL SECTION

All the chemicals were commercially purchased and used without further purification. In a typical experiment for preparing TiO_2 hollow spheres, heptahydrated zinc sulfate ($ZnSO_4 \cdot 7H_2O$, 0.48 g) was added to absolute ethanol (30 mL) under continuous stirring for 1 h to form a white suspension, and then, 2 mL of tetrabutyl titanate (TBT) was added into the suspension. The mixture was stirred for another hour and then transferred to a Teflon-lined autoclave (50 mL in volume) and solvothermally treated at 210 °C for 24 h. The resultant precipitate was washed thoroughly with ethanol and deionized water to remove the sulfates and other impurities. Finally, the as-prepared product was dried at 80°C overnight prior to being characterized. For synthesizing solid spheres, 2 mL of TBT was firstly dissolved in 30 mL of ethanol and then 0.48 g of $ZnSO_4 \cdot 7H_2O$ was added to the solution with stirring for 1 h to form a semitransparent suspension, followed by the same procedures described above.

The crystal structure and phase identification of the samples were performed by X-ray diffraction (XRD Bruker D8 ADVANCE) with a monochromatized source of Cu Kα1 radiation (λ = 0.15405 nm) at 1.6 kW (40 KV, 40 mA). A JEOL JSM-6510 scanning electron microscope (SEM) was used to investigate the morphologies of the samples. For field-emission transmission electron microscopy (TEM) observation, the samples were redispersed in ethanol by ultrasonic treatment and dropped on carbon−copper grids. TEM as well as high-resolution transmission electron microscopy (HRTEM) images were collected using a JEOL JEM 2100F microscope working at 200 kV and equipped with an energy-dispersive X-ray analyzer (EDX Oxford INCA Model 6498). The optical absorption characteristics of the powders were determined via a UV-vis diffuse reflectance spectrum (DRS) on a spectrophotometer (Hitachi U4100) equipped with an integrating sphere.

The photocatalytic activities of the TiO_2 spheres were evaluated by the photocatalytic degradation of a model pollutant methyl orange (MO) under visible light. A 500 W Xe lamp with a 420 nm cutoff filter was used as the light source, and a refrigerating water circuit was used to keep the reaction temperature at room temperature. The experiments were performed as follows: 250 mg of photocatalyst was added into a 250 mL MO solution (10 mg L^{-1}). Before illumination, the suspension was magnetically stirred for 1 h in the dark to reach the adsorption−desorption equilibrium between the MO and the photocatalyst. Then, the suspension was stirred and exposed to light irradiation. The concentrations of the MO were monitored by checking the absorbance at 464 nm during the degradation process using a Hitachi U-3010 UV-vis spectrophotometer.

3. RESULTS AND DISCUSSION

3.1. Intelligent Hydrated-Sulfate Template. In the proposed method, hydrated sulfate serves simultaneously as the spherical template, the water supplier, and the composition controller. It is

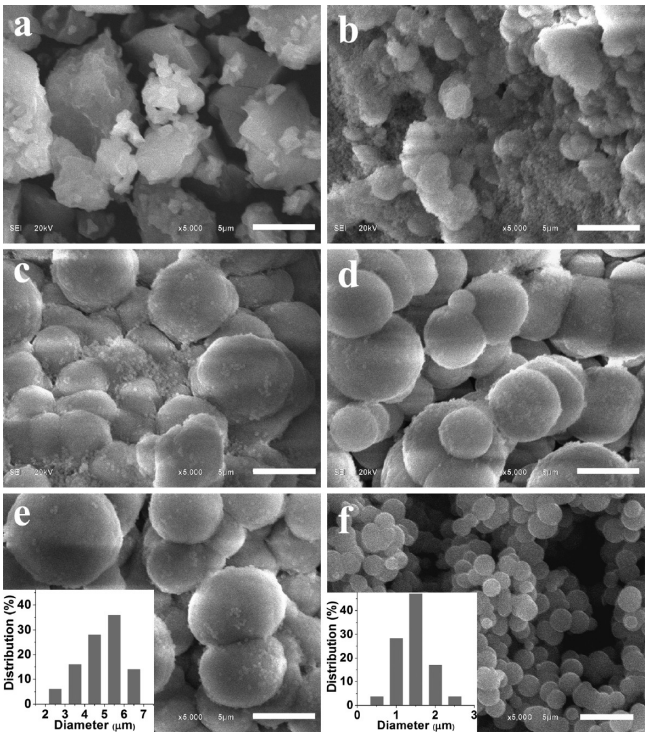

Figure 1. SEM images of (a) the raw $ZnSO_4 \cdot 7H_2O$ salt, (b−e) the stirred salt in ethanol for 5, 10, 30, and 60 min, and (f) the 60 min stirred salt in ethanol after the addition of TBT (scale bar 5 μm). The insets show the size distribution of the zinc sulfate templates before and after adding TBT.

observed that irregular hydrated sulfate powders of $MSO_4 \cdot xH_2O$ (M = Zn, Fe, Co, Mg, etc.) can be converted into spherical templates after stirring in ethanol. Namely, the self-conglobation effect during the stirring is the key to the formation of TiO_2 spheres. As illustrated in Figure 1a−e, the self-conglobation of the intelligent template was investigated carefully. Irregular hydrated sulfate (i.e., $ZnSO_4 \cdot 7H_2O$) powders gradually tend to be spherical to minimize their surface free energy during stirring in ethanol. After stirring for 10 min, the spheres of zinc sulfate have formed and become more regular as the stirring time increased. Stirring for more than 60 min, the suspension has been stable and the size of the spheres is unchanged, which makes the spheres easily repeatable in practical applications. After adding TBT into the sulfate suspension, the size of the spherical template decreased (Figure 1e,f). On the other hand, however, no spheres were observed when TBT was added to the ethanol before the additon of hydrated zinc sulfate, as shown in Figure S1a-b of the Supporting Information. Therefore, the order of the addition of the reactants is very important for the formation of hydrated sulfate spheres.

3.2. Structures and Morphologies of TiO_2 Spheres. The TiO_2 spherical sample was prepared by reacting TBT with the intelligent template, followed by solvothermal crystallization. When characterized by X-ray diffraction (XRD), all the diffraction peaks can be assigned to the anatase TiO_2 structure (JCPDS Card No. 21-1272), as shown in Figure 2a. The crystallite size of TiO_2 was calculated to be 8.5 nm using the Debye−Scherrer equation. The scanning electron microscopy (SEM) image shows a well-developed spherical morphology with a cavity inside (Figure 2b). The detailed structure of the spheres was revealed with the aid of TEM, as shown in Figure 2c,d. The TEM images

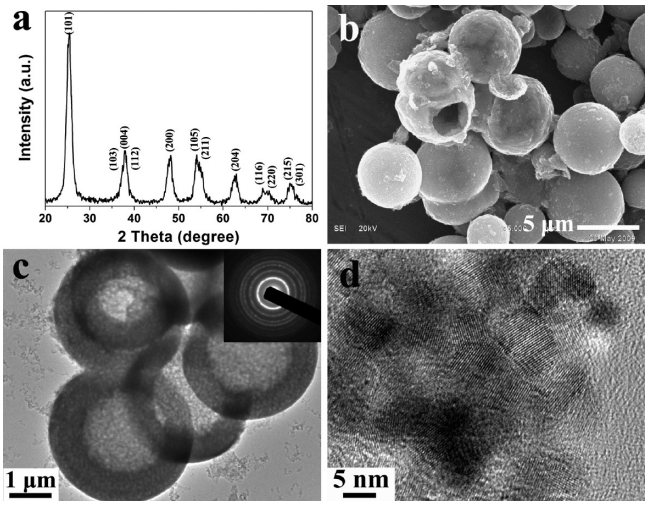

Figure 2. (a) XRD pattern and (b) SEM, (c) TEM, and (d) high-resolution TEM images of TiO_2 hollow spheres prepared using $ZnSO_4 \cdot 7H_2O$. The inset shows the selective area electronic diffraction (SAED) image.

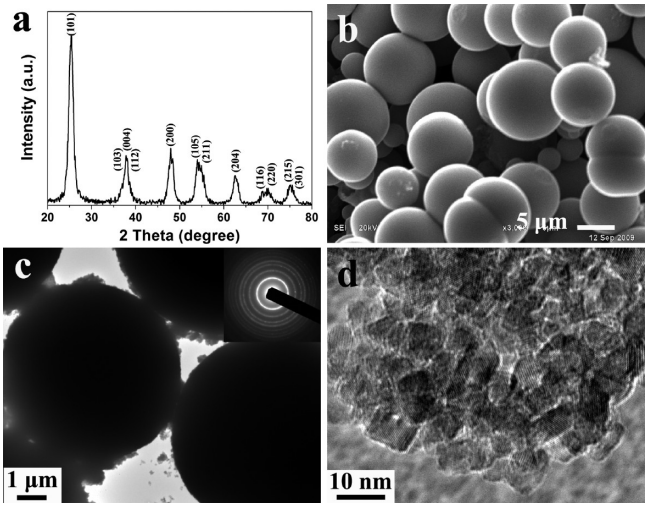

Figure 3. (a) XRD pattern and (b) SEM, (c) TEM, and (d) high-resolution TEM images of TiO_2 solid spheres. The inset shows the selective area electronic diffraction (SAED) image.

clearly demonstrate that the hollow shell structure consists of interconnected nanoparticles with a primary crystallite size of about 8 nm, and the nanoporosity in the shell is also evident from Figures 2c,d and S2 (Supporting Information; with the average pore size of 6.4 nm). The selective area electronic diffraction (SAED) image, as shown in the inset of Figure 2c, indicates that the nanocrystallites are random in orientation.

It is interesting that hollow or solid chamber structures can be controlled by adjusting synthesis procedure (altering the addition order of reactants). For the synthesis of TiO_2 solid spheres, 2 mL of TBT was first dissolved in 30 mL of ethanol and, then, 0.48 g of $ZnSO_4 \cdot 7H_2O$ was added to the solution with stirring for 1 h to form a semitransparent suspension, followed by the same procedures as described for hollow spheres. Figure 3 shows the XRD pattern and SEM and TEM images of the solid spherical anatase TiO_2 structure. The TEM image in Figure 3d indicates that the solid spheres consisting of highly crystallized TiO_2

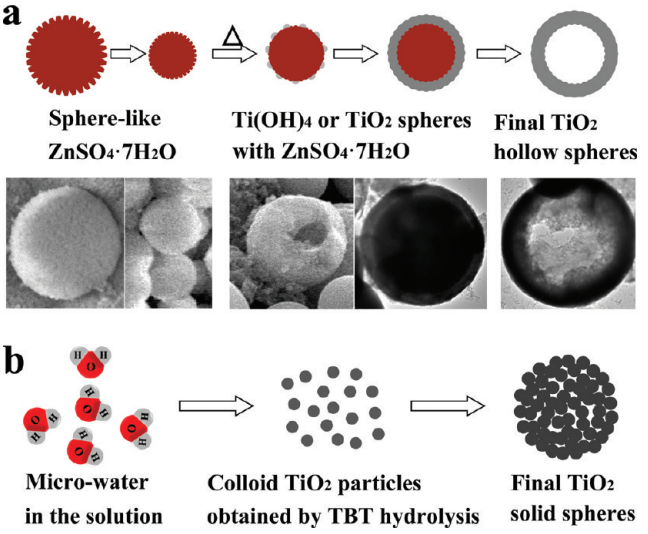

Figure 4. Schematic illustration of the formation mechanism of the two TiO_2 spheres. (a) Hollow spheres and the corresponding electron micrographs at different stages and (b) solid spheres.

nanocrystals are nanoporous structures. The crystallite size of the TiO_2 solid spheres, as determined from the anatase (101) peak using the Debye−Scherrer equation, was 9 nm, similar with the value obtained from high-resolution TEM image.

3.3. Growth Mechanism of TiO_2 Spheres. In order to understand the formation mechanism of the TiO_2 hollow spheres, we carried out the time-dependent experiments. Figure S3a−e (Supporting Information) shows SEM images depicting the structural evolution with reaction time. The images demonstrate that the spherical structure appeared at the early stage of growth and the size of the initial TiO_2 spheres is in line with that of zinc sulfate template after adding TBT. As shown in the insets of Figure S3 (Supporting Information), the average size of the spheres increased from 1.5 to 4.0 μm with the reaction progressing. The XRD patterns in Figure S3f (Supporting Information) further indicate the crystallinity development of TiO_2 spheres during crystal growth.

The formation of such hollow spheres involves the self-conglobation of metal hydrated sulfates ($MSO_4 \cdot xH_2O$, M = Zn, Fe, Co, Mg, etc.), the hydrolysis of tetrabutyl titanate ($Ti(OBu)_4$, TBT), and the subsequent solvothermal crystallization process. The self-conglobation of the intelligent template has been discussed above (Figure 1). The water was slowly released from hydrated sulfates. Subsequently, as shown in eqs 1−6, TBT was hydrolyzed at the surface of spherical hydrated sulfates, and the resulted TiO_2 colloid particles were accumulated to form spherical structure;[15] then, TiO_2 nanocrystallites were generated through the crystallization reaction under the solvothermal condition. The size of TiO_2 spheres obtained in the early growth stage is consistent with that of the spherical template after adding TBT; thus, the growth along the surface of templates is testified. As the system tries to lower its overall energy, nanocrystallites on the surface of a small particle tends to detach and diffuse through solution and, then, attach to the surface of a larger particle via the Ostwald ripening process.[16] Finally, the TiO_2 hollow spheres were obtained by removing templates during the washing process. As shown in Figure 4a, the formation process was observed, and the proposed mechanism was evidenced by the electron micrographs.

For the preparation of TiO_2 solid spheres, however, TBT was first dissolved in ethanol. Then, when the $ZnSO_4 \cdot 7H_2O$ was

added into the solution containing TBT, the hydrated sulfate should be surrounded immediately by TBT; thus, the self-conglobation of hydrated sulfates would be prohibited. SEM images in Figure S1a-b (Supporting Information), showing the irregular shape of the as-prepared zinc sulfate, justify the explanation above. On this occasion, as shown in Figure 4b, the microwater (water molecule) in the solution served as the nucleation center of TiO_2 and the obtained colloid particles were accumulated to form spheres to lower the overall energy. At last, the anatase TiO_2 solid spheres were formed after the solvothermal reaction.

Considering together the formation of both hollow and solid spheres, we propose that there are two competitive mechanisms in the system, the hydrated-sulfate induced process and the microwater induced process. Namely, for the hollow sphere preparation, in the existence of spherical sulfates, the hydrated-sulfate induced mechanism plays the dominant role. Whereas, for preparing solid spheres, the microwater induced mechanism dominates. In order to prove this statement, extra experiments were carried out. Before the solvothermal reaction, the sulfates were centrifugalized and removed from the white suspension (semitransparent suspension) for preparing hollow spheres (solid spheres). The supernatants were solvothermally treated, and only the solid spheres could be obtained in both synthetic procedures. As shown in Figure S1c-d (Supporting Information), the results provide direct evidence for the growth mechanisms discussed above, which is because there is only microwater in the solution.

$$\mathrm{Ti(OBu)_4 + H_2O \rightarrow (BuO)_3TiOH + BuOH} \quad (1)$$

$$\mathrm{(BuO)_3TiOH + H_2O \rightarrow (BuO)_2Ti(OH)_2 + BuOH} \quad (2)$$

$$\mathrm{(BuO)_2Ti(OH)_2 + H_2O \rightarrow BuOTi(OH)_3 + BuOH} \quad (3)$$

$$\mathrm{BuOTi(OH)_3 + H_2O \rightarrow Ti(OH)_4 + BuOH} \quad (4)$$

$$\equiv \mathrm{TiOBu + HOTi} \equiv \rightarrow \equiv \mathrm{TiOTi} \equiv + \mathrm{BuOH} \quad (5)$$

$$\equiv \mathrm{TiOH + HOTi} \equiv \rightarrow \equiv \mathrm{TiOTi} \equiv + \mathrm{H_2O} \quad (6)$$

The wall thickness for hollow structures is a key parameter being concerned with their properties. It is worth noting that the wall thickness of the hollow spheres can be easily tailored by adjusting the concentration of TBT. In the above experiments, the concentration of TBT added into the suspension is 100 vol %. In order to tune the wall thickness, the TBT concentration is diluted to 50 and 20 vol % with ethanol before addition. As shown in Figure 5, the wall thickness of TiO_2 spheres decreases gradually with the reduction of TBT concentration. More broken spheres can be observed in the samples due to their low strength of the thinner shells. Additionally, rough internal surface of the spheres is corresponding to the rough surface of spherical $ZnSO_4 \cdot 7H_2O$ template, which provides additional evidence for the proposed growth mechanism.

3.4. Generality of the HAS Strategy. The synthesis strategy presented here that provides a simple approach for in situ one-step preparation of TiO_2 spheres with tunable structures can be widely applied to other systems. The TiO_2 spheres would be synthesized in various solvents using different hydrated sulfates.

Figure 6 shows the XRD patterns and SEM images of TiO_2 spheres prepared in various alcohols using $ZnSO_4 \cdot 7H_2O$. All the samples possess the anatase TiO_2 structure and have a

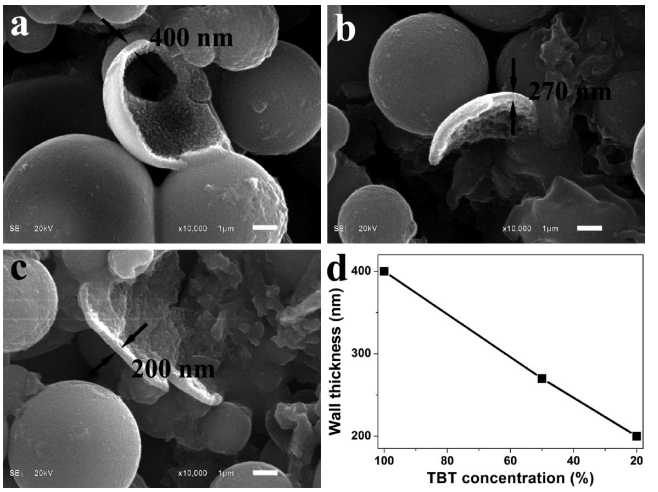

Figure 5. SEM images of TiO_2 hollow spheres with different wall thicknesses obtained from various tetrabutyl titanate (TBT) concentrations: (a) 100 %, (b) 50 %, and (c) 20%; (d) thickness variation with TBT concentrations (scale bar 1 μm).

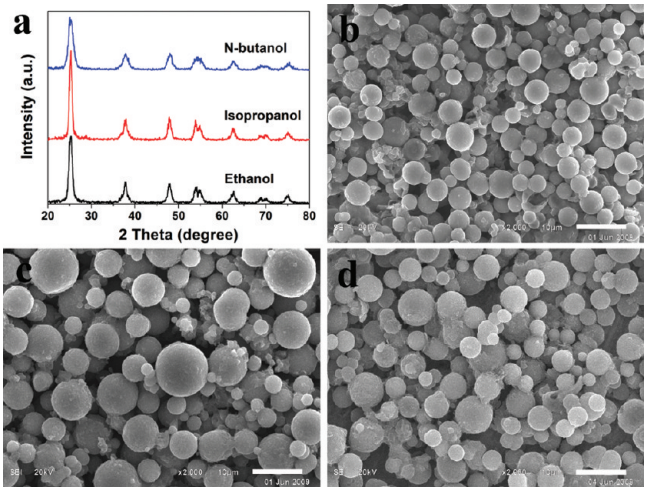

Figure 6. XRD patterns (a) and SEM images of the TiO_2 spheres prepared in various solvents: (b) ethanol, (c) isopropanol, and (d) *n*-butanol (scale bar 10 μm).

well-developed spherical morphology. Furthermore, the crystallinity of nanoparticles can be easily controlled by varying the solvent with different dielectric constant, well-consistent with our previous report.[17] In addition, titanium tetra-isopropoxide (TTIP) is available to replace TBT, and anatase TiO_2 spheres can also be obtained by employing this HAS strategy (see Figure S4 in Supporting Information).

It has been proven that the TiO_2 spheres prepared using $ZnSO_4 \cdot 7H_2O$ have a hybrid composition with ZnO.[14] When other hydrated sulfates ($FeSO_4 \cdot 7H_2O$, $CoSO_4 \cdot 7H_2O$, $MgSO_4 \cdot 7H_2O$, etc.) were employed, spheres of TiO_2 having different compositions with various colors were successfully prepared by adopting this strategy (Figure 7). These microsphere products all display an XRD pattern characteristic of anatase TiO_2 with rather similar morphology (Figure 8). When TiO_2 spheres synthesized using $FeSO_4 \cdot 7H_2O$ (denoted as TiO_2/Fe_2O_3) were taken as the example, the detailed structure was further investigated by the TEM analysis. As shown in Figure 9a,b, the results indicate that

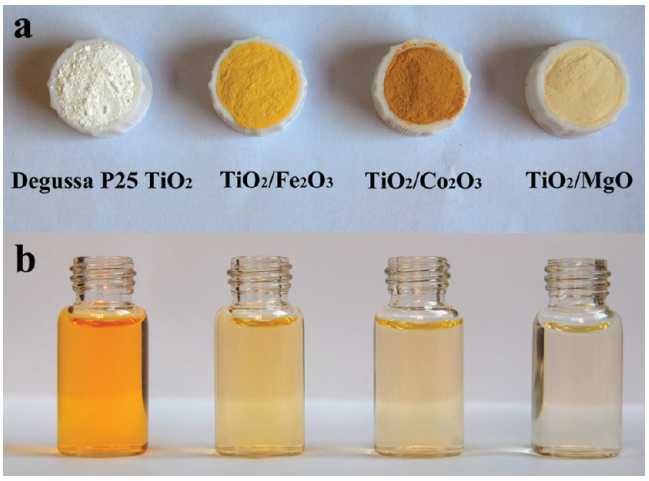

Figure 7. Photographs of (a) the hybrid TiO_2 spheres with different compositions and P25; (b) the corresponding MO photocatalytic degradation performance.

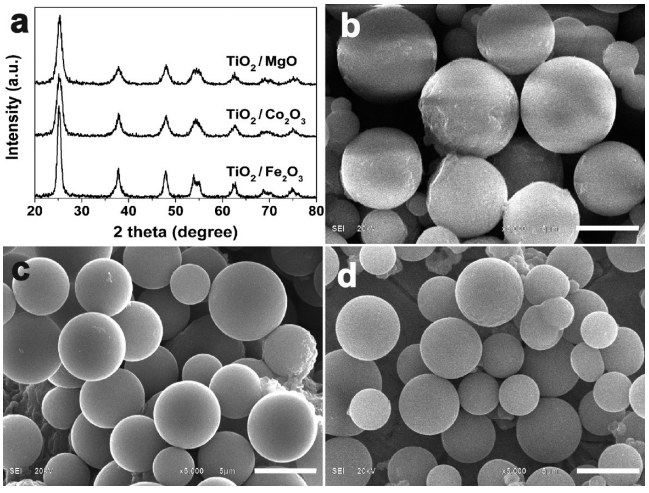

Figure 8. (a) XRD patterns of the hybrid TiO_2 spheres with different compositions and the corresponding SEM images: (b) TiO_2/Fe_2O_3, (c) TiO_2/Co_2O_3, and (d) TiO_2/MgO (scale bar 5 μm).

the hybrid TiO_2 spheres consist of interconnected nanoparticles with a primary size of about 10 nm and exhibit a nanoporous structure. The selected area electron diffraction (SAED) image (Figure 9c) indicates that the nanocrystallites are random in orientation. Energy-dispersive X-ray spectroscopy (EDS) shown in Figure 9d determines the Fe content in the product to be 2.3 atomic %. Further evidence for the existence of Fe_2O_3 was obtained from the UV-vis diffuse reflectance spectrum in Figure 10a, from which two absorption edges corresponding to TiO_2 (at 420 nm) and Fe_2O_3 (at 550 nm) were observed. It should be pointed out that a red shift of the absorption edges for TiO_2 was observed, due to a small amount of Fe^{3+} ions doped into the TiO_2 lattice. Thus, the structure of the "hybrid" material is the composite of M-doped TiO_2 and MO_x (M = Fe, Co, Mg, etc.). As shown in Figure 10a, the hybrid TiO_2 spheres exhibit significant absorption in the visible region (except for the TiO_2/ZnO spheres which are an excellent UV-light-driven photocatalyst); therefore, they are expected to possess visible-light photocatalytic abilities.

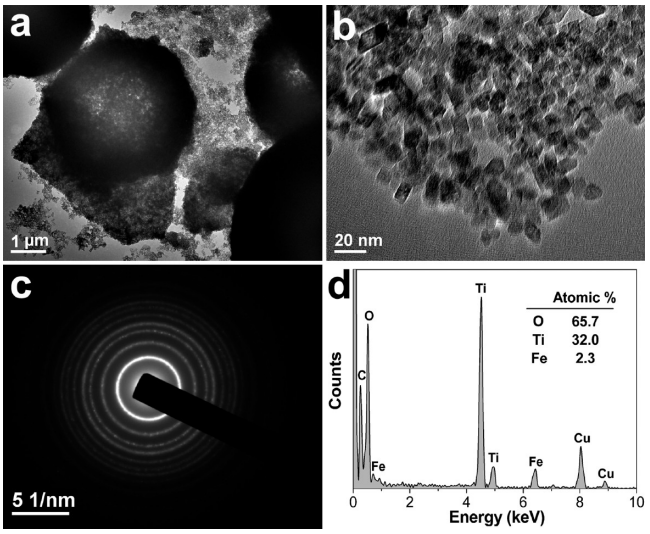

Figure 9. (a,b) TEM images, (c) selective area electronic diffraction (SAED) image, and (d) energy-dispersive X-ray spectroscopy (EDS) of the as-prepared TiO_2/Fe_2O_3 spheres.

3.5. Photocatalytic Activities. The photocatalytic activities of the hybrid TiO_2 spherical samples were evaluated by degrading a widely used dye, MO, under visible-light (λ > 420 nm) irradiation. Figure 10b shows the photocatalytic performance of the hybrid TiO_2 spheres with different compositions. A blank test (MO without any catalyst) exhibits almost no photolysis, and MO over Degussa P25 shows little photodegradation, while as-prepared hybrid TiO_2 spheres present prominent photocatalytic activities under visible-light irradiation. After irradiation for 24 h, the MO degradation efficiencies reach 90%, 80%, and 72% for TiO_2/MgO, TiO_2/Co_2O_3 and TiO_2/Fe_2O_3 spheres, respectively. In addition, photocatalytic experiments under UV light were also carried out, and the results are shown in Figure S5 (Supporting Information). These results provide further evidence that only very few metallic ions dope into the TiO_2 lattice, because heavy doping should drastically degrade the photocatalytic performance. The excellent performance of the hybrid TiO_2 spheres is attributed to the heterojunctions constituted of TiO_2 and the hybridized metal oxides.[18] As shown in Figure S6 (Supporting Information), for TiO_2/Fe_2O_3 spheres, the light absorption occurred in both Fe-doped TiO_2 and Fe_2O_3. The electrons in the valence band (VB) are excited to their conduction band (CB) and left the holes in the VB under visible-light illumination. Due to the favorable energy bias between the two sides of the Fe_2O_3 and TiO_2, the photo-generated carriers separate readily at the heterojunctions. Thus, the probability of electron-hole recombination can be reduced. The separated carriers can participate in photocatalytic reactions to directly or indirectly mineralize organic pollution, resulting in the enhanced photocatalytic activity. The photocatalytic process of TiO_2/Co_2O_3 spheres is similar with that of TiO_2/Fe_2O_3 spheres. Therefore, using the present approach, it is possible to further improve the photocatalytic performance by optimizing the composition of hybrid microspheres.

While for TiO_2/MgO spheres, MgO has no contribution to visible-light absorption and detailed research is further required to understand the visible-light photocatalytic activity. We propose that a part of Mg^{2+} goes into the TiO_2 lattice and some defect levels are introduced in the forbidden bandgap. In this system, the oxygen vacancies are generated according to eq 7 and play a

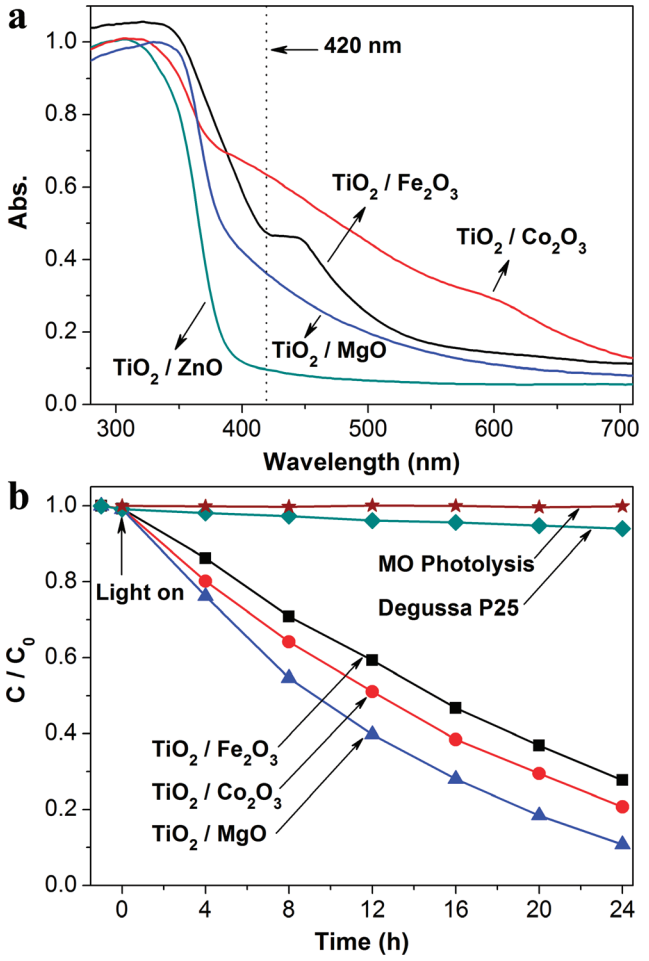

Figure 10. (a) UV-vis diffuse reflectance spectra of the hybrid TiO_2 spheres; (b) MO photocatalytic degradation over the TiO_2/Fe_2O_3 spheres (■), TiO_2/Co_2O_3 spheres (●), TiO_2/MgO spheres (▲), Degussa P25 TiO_2 (♦), and without catalyst (★) under visible-light irradiation.

dominant role for visible-light absorption of TiO_2/MgO spheres (Figure S7, Supporting Information). Postheat treatment of TiO_2/MgO spheres was carried out to verify this statement. As shown in Figure S8 (Supporting Information), no visible spectral response can be observed for the sample after calcination at 550°C in air, owing to the disappearance of oxygen vacancies after calcination. Correspondingly, almost no visible-light photocatalytic activity was observed (Figure S9, Supporting Information).

$$MgO \xrightarrow{TiO_2} Mg''_{Ti} + O_O^x + V_O^{\bullet\bullet} \qquad (7)$$

4. CONCLUSION

In summary, an intelligent-template strategy, based on a hydrated-sulfate assisted solvothermal (HAS) process, is demonstrated to be simple and powerful for preparation of TiO_2 spheres. The as-prepared anatase TiO_2 sphere has a hierarchical structure: the sphere is several micrometers in size, the shell consists of interconnected TiO_2 nanoparticles, and there is a nanoporous network between TiO_2 nanocrystals. The hybrid TiO_2 spheres exhibit good photocatalytic activities under visible-light irradiation. The method has been demonstrated to be applicable to various solvents, titanium sources, and different hydrated-sulfates. Furthermore, the wall thickness and interior structures are easily controlled by altering Ti precursor concentration and synthetic procedure. The strategy, thus, can be considered as a general route to achieve nanoporous TiO_2 spheres with tunable structures and various compositions. The advantages of the strategy lie in the following: (i) this is a very simple and cost-effective route using hydrated sulfates both as the template and the water supplier, and the sulfates can be easily removed by washing; (ii) the wall thickness, chamber structure, and composition of the products can be easily tailored by simply varying the starting reactants and synthesis procedure; (iii) this method can be widely applied in many systems; and (vi) all of the starting materials are earth abundant and environmentally benign. With all these virtues, it would be a quite prosperous way to fabricate nanoporous metal oxide with controllable structures and compositions.

■ ASSOCIATED CONTENT

Supporting Information. SEM images of irregular $ZnSO_4 \cdot 7H_2O$ and TiO_2 solid spheres, nitrogen adsorption−desorption isotherm, SEM images of the TiO_2 products evolving with reaction time, XRD pattern and SEM images of TiO_2 spheres prepared using titanium tetra-isopropoxide (TTIP), MO photocatalytic degradation over the hybrid TiO_2 spheres under UV light irradiation, the schematic band structure of TiO_2/Fe_2O_3 and TiO_2/MgO spheres, UV-vis diffuse reflectance spectra and MO photocatalytic degradation of the TiO_2/MgO spheres before and after calcination under visible-light irradiation. This material is available free of charge via the Internet at http://pubs.acs.org.

■ AUTHOR INFORMATION

Corresponding Author

*E-mail: huangfq@mail.sic.ac.cn. Tel: +86-21-5241-1620. Fax: +86-21-5241-6360.

■ ACKNOWLEDGMENT

This work is financially supported by National 973 Program of China Grant Nos. 2007CB936704 and 2009CB939903, National Science Foundation of China Grant Nos. 50772123 and 50821004, and Science and Technology Commission of Shanghai Grant Nos. 0752 nm016, 0952 nm06500 and 08JC1420200. The authors thank Dr. Yin Xin, Yaoming Wang, Dongyun Wan, and Ms. Shan Guo for their helpful suggestions.

■ REFERENCES

(1) Fujishima, A.; Honda, K. *Nature* **1972**, *238*, 37–38.
(2) O'Regan, B.; Gratzel, M. *Nature* **1991**, *353*, 737–740.
(3) Li, Y. Z.; Kunitake, T.; Fujikawa, S. *J. Phys. Chem. B* **2006**, *110*, 13000–13004.
(4) Kondo, Y.; Yoshikawa, H.; Awaga, K.; Murayama, M.; Mori, T.; Sunada, K.; Bandow, S.; Iijima, S. *Langmuir* **2007**, *24*, 547–550.
(5) Yang, S.; Yang, D.; Kim, J.; Hong, J.; Kim, H.; Kim, I.; Lee, H. *Adv. Mater.* **2008**, *20*, 1059–1064.
(6) Kim, S.-W.; Kim, M.; Lee, W. Y.; Hyeon, T. *J. Am. Chem. Soc.* **2002**, *124*, 7642–7643.
(7) Kamata, K.; Lu, Y.; Xia, Y. *J. Am. Chem. Soc.* **2003**, *125*, 2384–2385.
(8) Liang, H. P.; Zhang, H. M.; Hu, J. S.; Guo, Y. G.; Wan, L. J.; Bai, C. L. *Angew. Chem., Int. Ed.* **2004**, *43*, 1540–1543.

(9) Wang, Y.; Zhou, A.; Yang, Z. *Mater. Lett.* **2008**, *62*, 1930–1932.
(10) Walsh, D.; Lebeau, B.; Mann, S. *Adv. Mater.* **1999**, *11*, 324–328.
(11) Eun, T. H.; Kim, S.-H.; Jeong, W.-J.; Jeon, S.-J.; Kim, S.-H.; Yang, S.-M. *Chem. Mater.* **2009**, *21*, 201–203.
(12) Li, X.; Xiong, Y.; Li, Z.; Xie, Y. *Inorg. Chem.* **2006**, *45*, 3493–3495.
(13) Zhang, S.; Liu, C.; Liu, Y.; Zhang, Z.; Li, G. *J. Am. Chem. Soc.* **2008**, *91*, 2067–2070.
(14) Lü, X. J.; Huang, F. Q.; Mou, X. L.; Wang, Y. M.; Xu, F. F. *Adv. Mater.* **2010**, *22*, 3719–3722.
(15) Fei, H.; Liu, Y.; Li, Y.; Sun, P.; Yuan, Z.; Li, B.; Ding, D.; Chen, T. *Microporous Mesoporous Mater.* **2007**, *102*, 318–324.
(16) Yang, H. G.; Zeng, H. C. *J. Phys. Chem. B* **2004**, *108*, 3492–3495.
(17) Wu, J. J.; Lü, X. J.; Zhang, L. L.; Huang, F. Q.; Xu, F. F. *Eur. J. Inorg. Chem.* **2009**, *2009*, 2789–2795.
(18) Bessekhouad, Y.; Robert, D.; Weber, J. V. *Catal. Today* **2005**, *101*, 315–321.